Cerebral Cortex February 2010;20:257–270
doi:10.1093/cercor/bhp096
Advance Access publication May 14, 2009

Cortical Connections to Area TE in Monkey: Hybrid Modular and Distributed Organization

Elena Borra[1,2], Noritaka Ichinohe[2], Takayuki Sato[3], Manabu Tanifuji[3] and Kathleen S. Rockland[2]

[1]Dipartimento di Neuroscienze, Sezione di Fisiologia, Università di Parma; Istituto Italiano di Tecnologia (IIT, Unità di Parma), I43100 Parma, Italy, [2]Laboratory for Cortical Organization and Systematics, Brain Science Institute, RIKEN, 2-1 Hirosawa, Wako-shi, Saitama 351-0198, Japan and [3]Laboratory for Integrative Neural Systems, RIKEN Brain Science Institute, Wako-shi, Saitama 351-0198, Japan

To investigate the fine anatomical organization of cortical inputs to visual association area TE, 2–3 small injections of retrograde tracers were made in macaque monkeys. Injections were made as a terminal procedure, after optical imaging and electrophysiological recording, and targeted to patches physiologically identified as object-selective. Retrogradely labeled neurons occurred in several unimodal visual areas, the superior temporal sulcus, intraparietal sulcus (IPS), and prefrontal cortex (PFC), consistent with previous studies. Despite the small injection size (<0.5 mm wide), the projection foci in visual areas, but not in IPS or PFC, were spatially widespread (4–6 mm in extent), and predominantly consisted of neurons labeled by only one of the injections. This can be seen as a quasi-modular organization. In addition, within each projection focus, there were scattered neurons projecting to one of the other injections, together with some double-labeled (DL) neurons, in a more distributed pattern. Finally, projection foci included smaller "hotspots," consisting of intermixed neurons, single-labeled by the different injections, and DL neurons. DL neurons are likely the result of axons having extended, spatially separated terminal arbors, as demonstrated by anterograde experiments. These results suggest a complex, hybrid connectivity architecture, with both modular and distributed components.

Keywords: branched collaterals, double-labeled neurons, modularity, object recognition, optical imaging

Introduction

Inferotemporal cortex (IT; area TE) in macaque monkeys is closely associated with visual object recognition (e.g., Logothetis et al. 1995; Tanaka 1996; Tsao et al. 2003). Beyond this well-documented fact, however, questions and controversies abound (Logothetis 2000; Pasupathy 2006; Bell et al. 2009; Orban 2008). According to one proposal, neural response properties in area TE are viewed as built-up by a convergence of inputs from early, unimodal visual cortical areas (V4, TEO, posterior TE [TEp]) (Kobatake and Tanaka 1994). Other investigators have emphasized a distributed network, where object recognition in TE is considered as integrated with activity in several other areas (Haxby et al. 2000; Fairhall and Ishai 2007). Another proposal, generating considerable recent interest, is that there are several functionally specialized modules, and that these form separable, interlinked subsystems (Tsao and Livingstone 2008). Electrical microstimulation, combined with functional magnetic resonance imaging (fMRI) in monkeys, has demonstrated 6 interconnected patches responsive to face stimuli: 2 distinct patches in anterior TE and 4 additional patches in posterior areas likely to project to TE: area TEO, posterior TE, and the fundus and lower lip of the superior temporal sulcus (STS) (Moeller et al. 2008).

The anatomical connections of TE have been extensively investigated. These chiefly include inputs from retinotopically organized posterior visual areas, and identified areas within the STS, intraparietal sulcus (IPS), and prefrontal cortex (PFC) (Morel and Bullier 1990; Baizer et al. 1991; Webster et al. 1991, 1994; Martin-Elkins and Horel 1992; Felleman et al. 1997; Saleem et al. 2000, 2008; Ungerleider et al. 2008). There are also dense connections with perirhinal cortex (Webster et al. 1991; Suzuki and Amaral, 1994; Saleem and Tanaka 1996; Lavenex et al. 2002). This anatomical distribution is generally consistent with data from fMRI and physiological experiments. Previous retrograde tracing experiments, however, have used large injections. These would be unlikely to reveal fine scale, modular organization. Earlier studies in fact have not reported any obvious clustering of retrogradely labeled afferent neurons after tracer injections in TE. This contrasts with the pronounced modularity of feedforward connections between areas V1 and V2 (Livingstone and Hubel, 1984, 1987; Sincich and Horton, 2002) and V2 and V4 (Rockland and Pandya, 1981; Shipp and Zeki, 1985; Zeki and Shipp, 1989; Ungerleider et al. 2008). One report of injections in posterior IT cortex has described multiple clusters of labeled cells within V4 (Felleman et al. 1997).

In the present experiments, we set out to determine whether cortical inputs to TE exhibited any discernible anatomical modularity. We used small injections (300–500 μm), comparable in size to optically imaged activity spots in TE (Tsunoda et al. 2001), and multiple, color-distinguishable retrograde tracers targeted to specific activity spots (Fig. 1). Injected tracers were cholera toxin (CTB), conjugated to Alexa488 (green fluorescence), Alexa555 (red fluorescence), or gold nanoparticles (silver enhanced reaction product). For the sake of simplicity, the respective labeled neuron populations will be referred to as "green", "red," and "silver".

This protocol resulted in several new results. 1) Connections from posterior visual areas (feedforward) were confirmed as conspicuously widespread (over 4–6 mm), despite the small size of the injections. 2) Predominantly, projection foci were organized in large swaths labeled by one of the injections (red, green, or silver), but embedded within these were scattered neurons labeled by one of the other injections. 3) Projection foci contained smaller zones ("hotspots") where neurons projecting to different injection sites were intermixed, along with some double-labeled (DL) neurons. 4) In marked contrast, projections from the IPS and PFC formed small patches. Labeled neurons within these tended to be intermixed (rather than segregated by injection site), including some DL neurons.

© 2009 The Authors
This is an Open Access article distributed under the terms of the Creative Commons Attribution Non-Commercial License (http://creativecommons.org/licenses/by-nc/2.0/uk/) which permits unrestricted non-commercial use, distribution, and reproduction in any medium, provided the original work is properly cited.

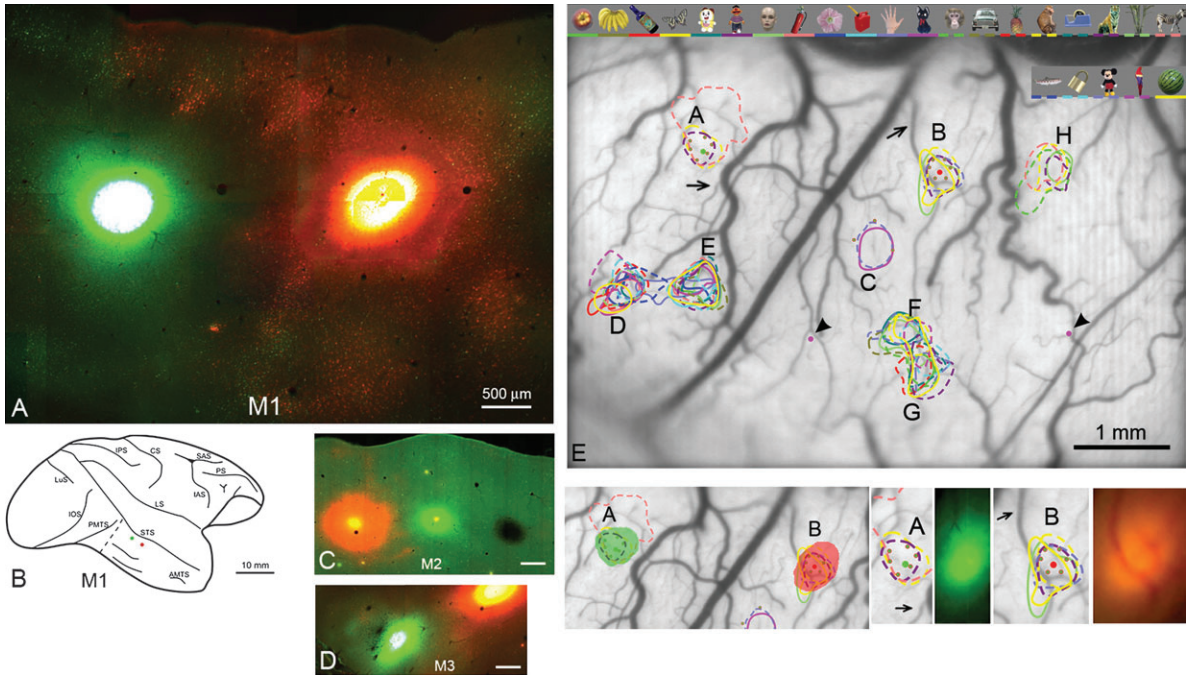

Figure 1. Photomicrographs (M1, M2, M3) of injection sites, and alignment (for M1) with optical-imaging patterns. (*A*) Fluorescence photomicrograph of the 2 injections (CTB-Alexa488, at left; CTB-Alexa555 at right) in M1. Note the clear separation of both injection cores and halo. The intense injection cores have saturated the optics and appear almost white. (*B*) Schematic brain diagram to show the location of the 2 injections in M1. Dashed line anterior to PMTS indicates the border between the tangentially sectioned block (containing the injection sites) and the larger, coronally sectioned posterior block. (*C*, *D*) Photomicrographs of the 3 injections in M2 and of 2 of the 3 injections in M3, at slightly lower magnification (and see Figs 3 and 7 for schematic brain diagrams). (*E*) Photograph of the brain surface (M1), seen through the implanted chamber. Note surface blood vessels, which were used as reference landmarks in the physiological experiments and guides for the anatomical injections. Eight regions (*A*–*H*) corresponding to surface darkening during the optical-imaging sessions are indicated. Colored outlines delineate domains responsive to the object stimuli shown at the top (and coded by a comparable color bar at the bottom of the image). Small green dots represent electrode penetrations. Large red and green dots in spots (*A*), (*B*) denote 2 injection sites. Purple dots (indicated by arrowheads, left and right of spot *F*) mark the position of DiI. Below left: The 2 anatomical injections are overlain (in solid green and solid red) on the 2 targeted (*A*, *B*) activity spots. Below right: Two pairs of images, showing activity spots (*A*) and (*B*) and the tracer injections, photographed in vivo, just subsequent to injection (see Methods). Arrows point to the same blood vessels as in (*E*). Scale bars in (*C*) and (*D*) = 500 µm. AMTS = anterior middle temporal sulcus; CS = central sulcus; IAS = inferior arcuate sulcus; LS = lateral sulcus; LuS = lunate sulcus; PMTS = posterior middle temporal sulcus; PS = principal sulcus; SAS = superior arcuate sulcus.

We interpret these results as indicating a complex connectivity architecture. Inputs from posterior visual areas to a given spot in TE are broadly convergent, but there is also divergence, as explicitly shown by the scattered neurons and small "hotspot" zones. Divergence is consistent with axon branching and multiple, spatially separate arbors, as demonstrated by anterograde tracing studies (Saleem et al. 1993). This would seem to best fit a hybrid organization, neither strictly distributed nor strictly modular. This general experimental design, of distinguishable small injections, can be useful in further investigations of physiologically characterized domains and their connectivity.

Table 1
Experimental history (dates of optical-imaging and electrophysiology sessions, tracer injections, and perfusion) of M1, M2, and M3

Monkey	M1 (R127)	M2 (R139)	M3 (R138)
Weight and sex	6.5 kg male	4.5 kg male	6.0 kg male
Chamber implant	07.06.11, day 1	07.09.25, day 1	08.01.18, day 1
Optical imaging	07.06.19, day 9	07.10.02, day 8	08.01.25, day 8
	07.06.26, day 16	07.10.05, day 11	08.01.28, day 11
Electrophysiology	07.07.02, day 22	07.10.12, day 18	08.02.04, day 17
	07.07.06, day 26	07.10.15, day 21	08.02.08, day 22
	07.07.12, day 32	07.10.19, day 25	08.02.13, day 27
	07.07.19, day 39	07.10.26, day 32	08.02.19, day 31
	07.07.25, day 45	07.10.31, day 37	08.02.25, day 39
		07.11.19, day 56	08.02.29, day 43
		07.11.22, day 59	08.03.05, day 48
		07.12.03, day 70	08.03.10, day 53
		07.12.17, day 84	08.03.14, day 57
			08.03.19, day 62
			08.04.10, day 84
Injections	07.07.31, day 51	07.12.06, day 73	08.03.25, day 68
Tracers injected	CTB-Alexa488	CTB-Alexa488	CTB-Alexa488
	CTB-Alexa555	CTB-Alexa555	CTB-Alexa555
		CTB-gold	CTB-gold
Perfusion	07.08.13, day 64	07.12.18, day 85	08.04.11, day 85

Note: Italics indicate the electrophysiology sessions performed after tracers injections.

Methods

Three male Rhesus monkeys (*Macaca mulatta*) weighing 4.5, 6, and 6.5 kg were used in this study. All 3 animals were implanted with a head fixation post and recording chamber according to a previously described protocol (Wang et al. 1998; Sato et al. 2008). Briefly, a titanium chamber (diameter 22.5 mm) was fixed to the skull at the position corresponding to the dorsal part of area TE. Subsequently, 2 optical-imaging sessions, and 5–10 sessions of electrophysiological recording were carried out (see Table 1 and Supplementary Figs 1 and 2). These data will be reported in detail elsewhere (Sato et al., in preparation).

Three to 6 days after the last physiological experiment (or, next to last, in M2 and M3), animals were deeply anesthetized (i.m. ketamine, 11 mg/kg, followed by artificial ventilation with a mixture of N_2O [70%], O_2 [30%], and isoflurane [up to 1.5%]), and prepared for sterile surgery. All animal procedures were carried out in conformity with official Japanese regulations for research on animals, following institutionally approved protocols (RIKEN, Brain Science Institute), and in accordance with the US National Institutes of Health Guide for the Care and Use of Laboratory Animals (NIH Publication No. 80–23).

Tracer Injections

In M1, 2 retrograde tracers (cholera toxin subunit B conjugated with Alexa Fluor 488 [CTB-Alexa488; Invitrogen-Molecular Probes, Eugene, OR] and CTB conjugated with Alexa Fluor 555 [CTB-Alexa555; Invitrogen] were injected, and in M2 and M3, 3 tracers were injected [CTB-Alexa488, CTB-Alexa555, and CTB-colloidal gold conjugate, 7 nm {CTB-gold; List Biological Laboratories}]). Tracers were diluted, at 1% concentration, in 0.1 M phosphate-buffered saline (PBS), and 0.12-μL volumes were pressure injected through a 50-μm diameter glass micropipette attached to a 10-μL Hamilton syringe. Injection spacing is about 2-mm edge-to-edge, except that in M3 the center-to-center distance of CTB-Alexa488 and CTB-gold is about 0.9 mm. In all 3 animals, injection placement was guided, as was the electrophysiological recording, by the location of optically imaged spots referenced to the surface blood vessels (Fig. 1). Injections were made through a small slit in transparent artificial dura, previously placed in the chamber, to minimize brain pulsations.

After injections were completed, the injected field was photographed using Keyence (VB-G05) fluorescent stereomicroscopy (Fig. 1) to confirm successful delivery of tracers, and to assist in later alignment of injection sites with electrophysiological data. After recovery, there was one additional recording session for M2 and M3 (see Table 1).

Fixation and Tissue Preparation

After postinjection survival periods of 14 (M1), 13 (M2), and 18 days (M3), the monkeys were anesthetized with ketamine (11 mg/kg, i.m.) and Nembutal (overdose, 75 mg/kg i.p.), and perfused transcardially, in sequence, with saline containing 0.5% sodium nitrite (for 2 min), 4 L of 4% paraformaldehyde in 0.1 M phosphate buffer (PB; pH 7.4; 30 min), and chilled 0.1 M PB with 10%, 20%, and 30% sucrose. Brains were removed, and temporal cortex (area TE) containing the injection sites was separately trimmed for tangential sectioning, in order to assist enregistering the injection sites in relation to the physiological experiments. Enregistering the 2 data sets was done in relation to the surface blood vessel pattern, supplemented by 3 marker injections of DiI made just before the perfusion (Li et al. 2003).

After trimming, the TE blocks and remaining tissue were placed in 30% sucrose in PB for 2 days (at 4 °C). TE blocks were tangentially sectioned on a freezing microtome (at 50 μm) so that the brain surface and injection sites were parallel to the cutting plane, in a repeating series of 2 sections. In M1, one series was reacted by immunofluorescence to enhance the CTB-Alexa488 signal, and in M2 and M3, this designated series was double reacted for CTB-gold by silver-enhancement. The second series (of alternating sections) was only reacted by immunofluorescence to enhance the CTB-Alexa488 signal. For CTB-Alexa555, no enhancement was used.

The remaining, larger tissue blocks were cut coronally (at 50 μm) in a repeating series of 4 sections. In M1, one series (the first section of 4) was used to enhance the CTB-Alexa488 signal by immunofluorescence. In M2 and M3, this series was double-reacted for CTB-gold by silver-enhancement. The second of every 4 sections was stained for Nissl substance by thionin. The third of every 4 sections was reacted for CTB-Alexa488 by immunoperoxidase. The fourth section was reserved for other purposes, for subsequent staining as the first section, or was discarded. For M2, we processed a small series of sections in and around area TEO as an uninterrupted series for immunofluorescence (silver enhancement in the first section of 4), in order to assess clusters of green and red labeling more clearly.

Enhancement of CTB-Alexa488 Signal by Immunofluorescence

Sections were immunoblocked in 0.1 M PBS, pH 7.4, containing 0.5% Triton X-100 and 5% normal goat serum (PBS-TG) for 1 h at room temperature, and subsequently incubated with 1:1000 rabbit anti-Alexa488 antibody (Invitrogen) in PBS-TG for 2 days at 4 °C. After washing with 0.1 M PBS, sections were incubated for 1.5 h at room temperature in Alexa488-conjugated anti-rabbit polyclonal goat antibody (1:200; Invitrogen-Molecular Probes). To combine this procedure with visualization of CTB-gold (see next section), silver-enhancement for CTB-gold was performed first.

Visualization of CTB-gold by Silver Enhancement

Sections were washed with 0.1 M PB, followed by 0.01 M PB. The IntenSE M silver Enhancement kit (Amersham International; UK) was used to visualize CTB-gold signals (Sincich et al. 2007). A one-to-one cocktail of the IntenSE M kit solution and 33% gum arabic solution was used as a reagent. Development of reaction products was monitored under a microscope and terminated by rinsing the sections in 0.01 M PB and, subsequently, several rinses in 0.1 M PB. In general, incubation time was around 2 h.

Immunoperoxidase Reaction for CTB-Alexa488

To mitigate the problem of fading after prolonged light microscopic screening, immunoperoxidase reaction for CTB-Alexa488 was perfomed for the third section in the series. Sections were immunoblocked in PBS-TG for 1 h at room temperature, and subsequently incubated with 1:1000 rabbit anti-Alexa488 antibody in PBS-TG for 2 days at 4 °C. After washing with 0.1 M PBS, sections were incubated for 1.5 h at room temperature in biotinylated anti-rabbit polyclonal goat antibody (1:200; Vector Laboratories, Burlingame, CA) for 1.5 h at room temperature. Immunoreactivity was visualized by ABC incubation (one drop of reagents per 7 mL of 0.1 M PB, ABC Elite kits; Vector) followed by diaminobenzidine histochemistry with 0.03% nickel ammonium sulfate.

All sections were mounted on gelatin coated glass slides, air-dried, dehydrated in graded ethanol solutions, immersed in xylene, and coverslipped in DPX (Fluka, Buchs, Switzerland).

Data Analysis

Fluorescent signal was analyzed by using standard sets of filters: fluorescein (for CTB-Alexa488) or rhodamine (for CTB-Alexa555). CTB-Alexa488 and CTB-Alexa555 labeled neurons were identified by a green and red granular fluorescence in the cytoplasm, respectively. In the one section of each 4, reacted for CTB-gold, labeled cells were identified in dark field by the granular precipitate in the cytoplasm. In the coronal sections, the distribution of retrogradely labeled cells was analyzed and plotted in every 200 μm. Material was analyzed with a Nikon Eclipse E-800 microscope, at 100×–200×–400×, and chartings carried out by using Neurolucida, through a MicroFIRE digital camera incorporated in the microscope.

Injection size was defined according to previous studies (Luppino et al. 2003). The core of the injection site, that is the effective tracer uptake area, for CTB-Alexa488 and CTB-Alexa555 was considered to include the intensely fluorescent area around the needle track, and for CTB-gold was considered to be the densely stained regions adjacent to the needle track. Equivalence of tracer sensitivity was assessed, as part of another experiment, by injecting a mixture of CTB-Alexa488 and CTB-Alexa555 in the frontal lobe of one monkey. In this case, almost all neurons were DL (Ichinohe et al. 2008).

Identification of areas is not straightforward in the occipito-temporal region. There is considerable individual variability, and the borders between areas tend to be ambiguous or gradual (Boussaoud et al. 1991; Kobatake and Tanaka 1994; Zeki 1996). In identifying the location of projection foci, we have compared sulcal landmarks in our material with those of published physiologically and anatomically based maps (Seltzer and Pandya 1978; Yukie et al. 1990; Boussaoud et al. 1991; Saleem and Tanaka 1996). We have given only approximate retinotopic descriptions, because no visual field mapping was available from these monkeys.

In the frontal lobe, the PFC was subdivided according to Gerbella et al. (2007) and Carmichael and Price (1994). Inferior intraparietal areas were defined according to Blatt et al. (1990) and Borra et al. (2008).

To obtain a quantitative analysis of the cortical labeling observed in different cortical regions and areas, we counted the number of green, red, silver and DL or triple labeled neurons, as plotted in sections at 200 μm intervals, using Neurolucida software. In Tables 2 and 3, total numbers of labeled neurons are given by area or cortical region. The percentage of DL green/red neurons was calculated with respect to the total amount of labeled cells, adding the 2 tracers together (DL/tot) and then recalculated for each tracer separately (DL/g, DL/r). Calculations and tables were obtained with Microsoft Office Excel.

To generate a surface view representation of hotspot regions in the occipito-temporal cortex (Fig. 6), we first determined the anterior-posterior (AP) location of coronal sections (200 μm apart) on the photographed brain, with reference to sulcal changes. Then, relying on

Table 2

Quantitative analysis of retrogradely labeled neurons in the occipital and temporal cortex in M1 and M2

		IPa		r-ISTS (TEa)		c-ISTS		Crown (TEm)		TEOd-TEpd		TEOv		V4	
	TOT	Cells	%	Cells	%	Cells	%	Cells	%	Cells	%	Cells	%	Cells	%
M1															
Green	20 495	462	2.3%	3074	15.0%	1832	9.0%	452	2.2%	12 268	59.9%	527	2.6%	261	1.3%
Red	5794	986	17.0%	320	5.5%	168	2.9%	260	4.5%	4981	86.0%	41	0.7%	11	0.2%
DL	1257	100	8.0%	114	9.1%	50	4.1%	48	3.8%	925	73.6%	14	1.1%	3	0.2%
Tot	27 546	1548		3508		2050		760		18 174		582		275	
%DL/tot	4.6%	6.5%		3.2%		2.4%		6.3%		5.1%		2.4%		1.1%	
%DL/g	5.8%	17.8%		3.6%		2.7%		9.6%		7.0%		2.6%		1.1%	
%DL/r	17.8%	9.2%		26.3%		22.9%		15.6%		15.7%		25.5%		21.4%	
M2															
Green	14 689	559	3.9%	4388	30.1%	752	5.3%	3040	21.3%	4728	30.7%	174	1.2%	919	6.5%
Red	12 504	933	7.5%	1182	9.5%	281	2.2%	1646	13.2%	6113	48.9%	30	0.2%	1769	14.1%
DL	593	93	15.7%	84	14.2%	14	2.4%	166	28.0%	217	36.6%			15	2.5%
Tot	27 786	1585		5654		1047		4852		11 058		204		2703	
%DL/tot	2.1%	5.9%		1.5%		1.3%		3.4%		2.0%				0.6%	
%DL/g	3.9%	14.3%		1.9%		1.8%		5.2%		4.4%				1.6%	
%DL/r	4.5%	9.1%		6.6%		4.7%		9.2%		3.4%				0.8%	
Silver	1142			321	28.5%			603	52.4%	218	19.1%				
DL s + g	272			79				141		52					
DL s + r	50			5				21		25					
Triple	8							5		3					

Note: Total numbers and percentages are given by area or cortical region. % = percentage of one-color cells in one area or cortical region/total neurons of that color in the occipital and temporal cortex. Lower STS labeling was subdivided in rostral (r-ISTS) and caudal (c-ISTS); TEOv include labeling ventral to PMTS, clearly separated from the more densely labeled region dorsal to PMTS (TEp/TEO). It was not possible to define a border between TEp and TEO, so the quantitative analysis was performed for these 2 fields together.

%DL = The percentage of DL green/red neurons was calculated with respect to the total number of labeled cells, adding the 2 tracers (DL/tot) and for each tracer separately (DL/g, DL/r). In M2 silver cells were also counted (DLs + g = silver and green; DLs + r = silver and red).

sulcal landmarks and adjusting the magnifications, we re-mapped the location and extent in mm of the hotspots from the Neurolucida charting to the hemisphere schema.

Hotspot regions were first identified qualitatively. For several of these, a further quantitative analysis was carried out (Supplementary Fig. 4, and Supplementary Tables). A window of 1.5–2.0 mm, anchored to anatomical landmarks, was positioned on the supragranular layers so as to include both the hotspot region and surrounding cortex, in several adjacent sections. The window was then subdivided into bins of 100 μm, perpendicular to the pial surface, and for each bin the number of green, red and DL cells was calculated. Finally, for each bin 2 factors that were used to define the hotspot regions, were calculated: the ratio of red and green cells (secondary/primary color) and the percentage of DL. Calculations, table and graphs were obtained with Microsoft Office Excel.

Photographic Presentation

The photomicrographs shown in the present study were obtained by capturing images directly from the sections using a digital camera (AxioCam HRc, Zeiss, Germany) attached to the microscope (AxioScope 2 plus, Zeiss, Germany). Individual images were then imported into Adobe Photoshop (Adobe Systems Incorporated, San Jose, CA) so that they could be processed, eventually assembled into digital montages, and reduced to the final enlargement. In most cases, image processing required lighting, brightness, and contrast adjustments. These were matched to the real microscope image.

Results

Injection Sites: Physiology

In all 3 monkeys, the set of object stimuli resulted in multiple activity spots, as expected from previous studies (Wang et al. 1998; Tsunoda et al. 2001; Sato et al. 2008). Spots responding to at least 2 of 25 object stimuli were selected for further electrophysiological examination (see Table 1 and Supplementary Fig. 1). In those experiments, the multiunit activity (MUA) from within the spots was recorded in response to 100 object images. MUA responded variably to a range of object images over different categories (human face, water melon, tree, car, chair, etc.—see Sato et al. 2008 and Supplementary Fig. 2). Thus, under our experimental conditions, the activity spots were considered object selective, but not, or not strongly, face selective (Supplementary Figs 1 and 2; further detail and analysis will be given in Sato et al. in preparation).

Table 3

Quantitative analysis of retrogradely labeled neurons in the PFC in M1, M2 and M3

		Level a	Level b	Level c
M1				
	Tot PFC	12l	46-45A	45B-8/FEF
Green	205	152	45	15
Red	161	99	27	30
DL	44	37	6	1
Tot	410	288	78	46
%DL/tot	10.7%	12.8%	7.7%	2.2%
%DL/g	17.7%	19.6%	13.3%	6.7%
%DL/r	21.5%	27.2%	22.2%	3.3%
M2				
	Tot PFC	12r-12o	46-45A	45B-8/FEF
Green	338	139	135	64
Red	258	93	84	81
DL	37	5	19	13
Tot	688	251	279	158
%DL/tot	5.4%	2.0%	6.8%	8.2%
%DL/g	9.9%	3.5%	12.3%	16.9%
%DL/r	12.5%	5.1%	18.4%	13.8%
Silver	33	10	23	
DL s+g	8	3	5	
DL s+r	12	1	11	
triple	2		2	
M3				
	Tot PFC	12r	12l-45A	45B-8/FEF
Green	811	353	227	231
Red	348	81	207	60
DL	76	27	33	16
Tot	1235	461	467	307
%DL/tot	6.2%	5.9%	7.1%	5.2%
%DL/g	8.6%	7.1%	12.7%	6.5%
%DL/r	17.9%	25.0%	13.8%	21.1%

Note: Conventions as in Table 2.

Injection Sites: Anatomy

Tracer injections were made 3–6 days after the last physiological recording. Injection placement was guided, as was the electrophysiological recording, by the location of optically imaged spots, referenced to the surface blood vessels (Fig. 1). As evaluated histologically, 7 of the 8 injections were <500 μm in diameter (the anterior, red injection in M1 was slightly larger especially in the superficial layers, ~700 μm in diameter). Injections were defined as corresponding to the core region of uniformly dense labeling, distinguishable from the halo, where individual neurons could be discerned. In M3, the silver and green injections partially overlapped; this case was used mainly to confirm results in M1 and M2.

By comparison of injection sites and the optical-imaging map, we concluded that all injections successfully included the electrophysiological penetration sites. Agreement with the optically imaged spots was also excellent. However, as the borders of the spots were not sharp, especially when the results from multiple sessions were superimposed (Fig. 1), it is difficult to exactly overlay our injection sites with the individual optically imaged spots.

Because of the necessity of matching injection sites and optical-imaging data, the region around the injections sites was separately blocked and sectioned in the tangential plane. Perirhinal cortex and some tissue in the more anterior STS were thus not included in the coronal blocks and were not included in the analysis.

Posterior Visual Areas (V4, TEO, TEp)

In all 3 brains, labeled neurons occurred in posterior cortical areas consistent with previous reports (Morel and Bullier 1990; Baizer et al. 1991; Webster et al. 1991). These consisted of large projection foci which formed swaths of red or green neurons (Figs 2, 3). Silver neurons in M2 tended to form smaller patches (Fig. 3).

The swaths of neurons formed multiple large fields, each 4–6 mm AP and ML. We interpret these fields as corresponding to distinct visual areas, as previously defined by tracer experiments (Distler et al. 1993; Webster et al. 1991; Ungerleider et al. 2008) or visual field mapping (Baylis et al. 1987; Boussaoud et al. 1991). In particular, labeled neurons occurred in V4 in the vicinity of the inferior occipital sulcus (IOS; Figs 2, 3). Between the IOS and the posterior middle temporal sulcus (PMTS), the projection focus was very dense. In M1 (Fig. 2), the focus was reduplicated in 2 (sections *c* and *f*) or 3 (sections *d* and *e*). The 2 fields likely correspond to V4 and TEO (section e) or TEO and TEp more anteriorly (section *b*). The third anterior, dorsal field likely corresponds to TEm. In M2 (Fig. 3), multiple large patches were most pronounced anterior to PMTS (sections *b*, *c*, *d*). At this AP level, the likely correspondence is with ventral TEp, dorsal TEp, and TEm (adjacent to the STS). In M3, there was moderate label posterior, in what is probably V4, and dense label in the vicinity of the PMTS, in what is either TEO or TEp (not illustrated).

By using multiple injections, we were able to see some overall topography of the projection foci. This generally reflects the placement of the injection sites. Thus, the posterior injections produced projection foci situated more posterior to those resulting from the anterior injections. In M1, green neurons predominate posteriorly; and in M2, red neurons occur posteriorly. Green neurons intermix and then predominate anterior to the red focus. This trend was less obvious for the silver neurons, where patches of neurons were embedded in the predominantly green foci (Fig. 3, sections a–d). Topographic organization of connections has previously been reported, from TE to perirhinal cortex (Suzuki and Amaral 1994).

A possible topography was also suggested in comparing the 3 sets of injections. In M3, where injections were situated medial to those in M1, the position of the projection foci was ventrally offset relative to M1. M1 and M2 both had dorsally situated injections, but those in M2 were more anterior. Both brains had dense label in the zone between PMTS and STS; but at posterior levels (adjoining the IOS), the projection focus in M1 was ventrally offset relative to that in M2 (compare level *e*, *f* in Fig. 2 and *f* in Fig. 3).

Finer Scale Features

Closer examination of the large swaths of labeled neurons reveals several more detailed features. First, although the swaths were characterized by almost continuous labeling, some smaller patches could be detected (300–500 μm wide; arrowheads in Fig. 2*A*, sections *d* and *e*). In addition, single neurons frequently stood out in layer 2, and these tended to be separated by about 250 μm (arrows in Fig. 2*B*, arrowheads in Fig. 4*A*). Third, scattered neurons of the opposite color (i.e., projecting to a different injection site) consistently occurred within the larger swaths (Fig. 2*A*, hollow arrows in section *b* and *c* indicate red neurons in green patches). Fourth, in individual sections, it was common to find vertical rows of 4–7 closely aligned (i.e., touching) cells, horizontal rows of 4–5 closely aligned cells, and clumps of approximately 7 cells in close contact (Fig. 2*D* and Fig. 4*B*). In general, however, labeled cells were intermixed, without any apparent order, along with nonlabeled cells; and similarly, no clear organization was apparent when 2 single-labeled populations were intermixed (Fig. 2*D*).

Fifth and very striking, there were small islands ("hotspots"), within the swaths of green or red neurons, where the 2 colors were much less imbalanced (see "Quantitative" below, Methods, and Supplementary Tables and Fig. 4). Hotspots also usually contained DL neurons, and these tended to be more numerous than in the surrounding swath (Fig. 5 and Supplementary Fig. 4). The hotspots varied in size and shape. In posterior regions, these tended to be relatively small (0.5 × 0.5 mm or 0.8 × 1.0 mm), with a low density of labeled neurons (Fig. 5*A*). More anteriorly, in TEO, patches in individual sections aligned in a stripe-like configuration; and in TEp, they merged into one of the single-color projection foci (Fig. 6). The DL neurons can be assumed to have collateral branching to both injections. Single-colored intermixed neurons projected to one OR another injection. These neurons, however, may also have collateral branching, but in that case, collaterals would be to tissue not included in our injection sites (see Discussion).

Superior Temporal Sulcus

Multiple foci were prominent in the STS in all 3 brains (Figs 2, 3). These occurred from about the level of the anterior tip of the IOS and extended anteriorly. (Because the more anterior sections were included in a separate tissue block that was sectioned tangentially, these levels were not analyzed).

Concentrations of labeled neurons occurred posterior, in the lower bank and lip of the STS. This is likely to correspond to area FST (lower bank) and V4t (sulcal lip). Continuing anterior,

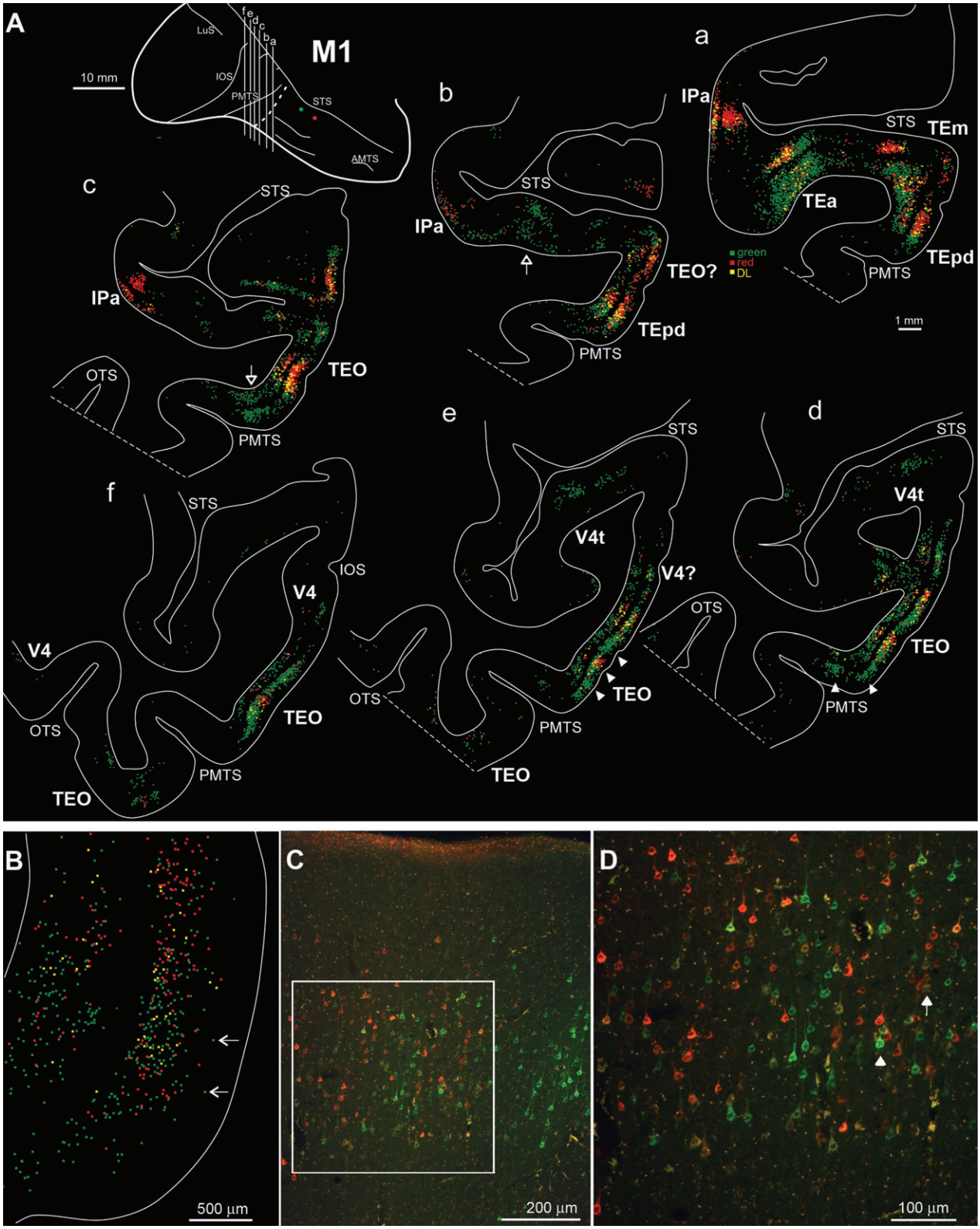

Figure 2. (*A*) Drawings of representative coronal sections showing the distribution of red, green, and DL (yellow) retrogradely labeled neurons in M1 in the occipito-temporal cortex. The black background is used to better visualize yellow, DL neurons. Each dot corresponds to one labeled neuron. Sections are in an anterior-to-posterior order (*a–f*). The different levels from which the sections were taken are indicated as lettered lines in the dorsolateral view of the injected hemisphere in the upper left part of the figure. Dashed lines (in white) on the hemisphere and on the section outlines correspond to a separate block, tangentially sectioned for injection site analysis. Hollow arrows in *b* and *c* indicate scattered red cells in green patches; arrowheads in sections d and e indicate single clusters of green, and of green and red cells in TEO. (*B*) Enlarged view of a labeled field from a section approximately at the level of section *b*. Arrows indicate neurons in layer 2 with a quasi-regular spacing. (*C*) Photomicrograph of a representative field of labeled neurons, from a section close to *b*. The white box indicates the region shown at higher magnification in (*D*). (*D*) Arrowhead indicates a tight clump of 4 cells and the arrow indicates a vertical row of neurons (see "Fine scale," in the text). OTS = occipito-temporal sulcus. Other abbreviations as in Figure 1.

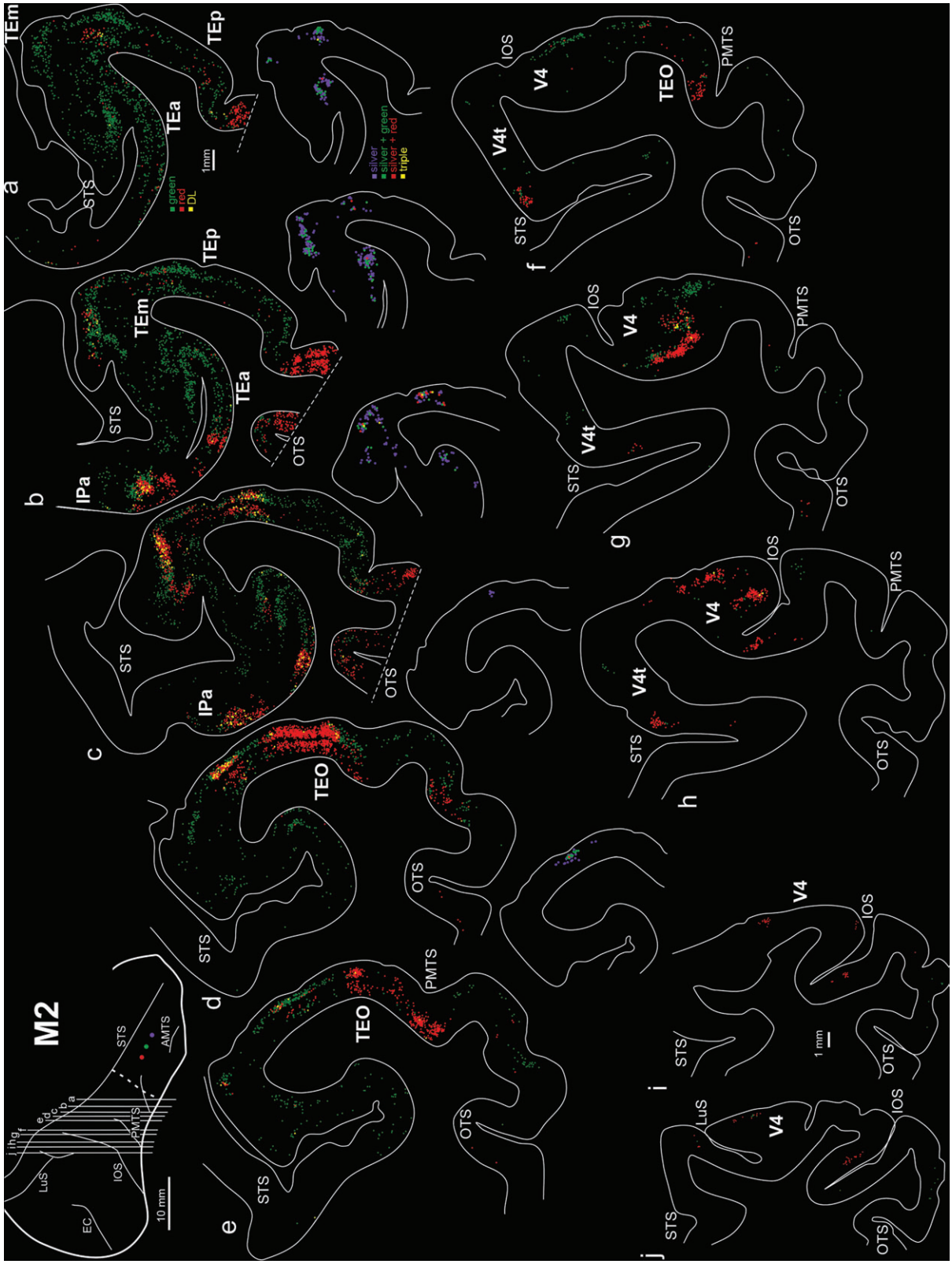

Figure 3. Drawings of representative coronal sections showing the distribution of red, green, silver, and DL (from red and green injections) retrogradely labeled neurons in M2 in the occipito-temporal cortex. Sections are in an anterior-to-posterior order (*a–j*). For sections *a–e*: the larger sections are used to show red, green and DL red + green (yellow) neurons; the smaller, partial sections separately show silver (purple), DL silver + green (green), silver + red (red), and triple silver + red + green (yellow) labeled neurons. Scale bar in *a* applies to sections *a–h*; Scale bar in *i* applies also to *j*. Conventions and abbreviations as in Figures 1 and 2.

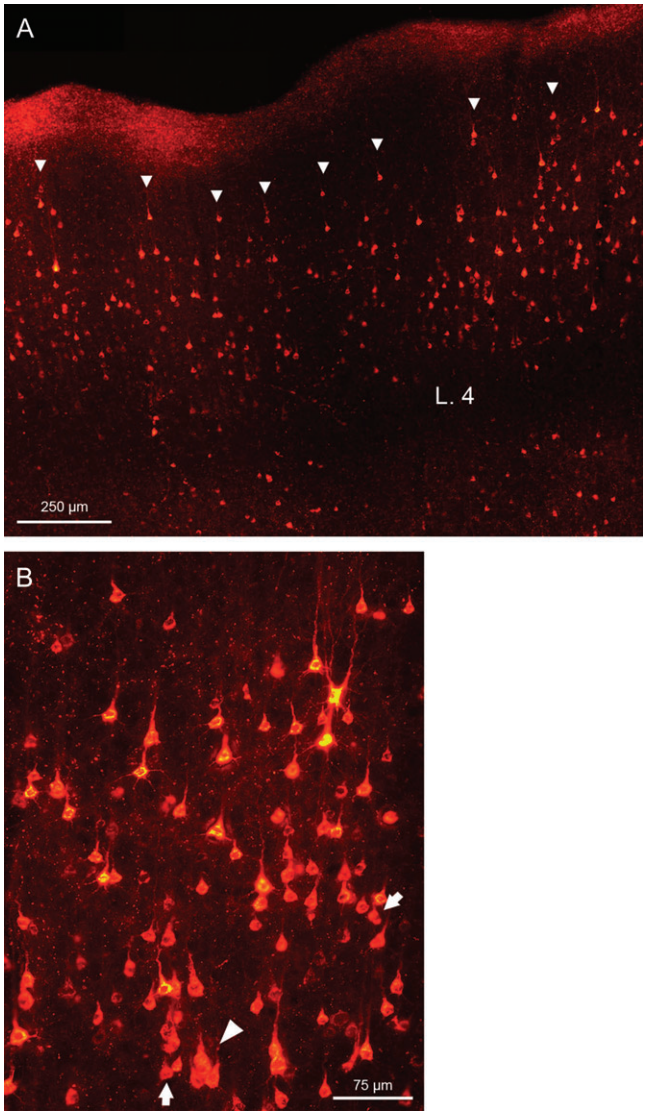

Figure 4. Photomicrographs illustrating finer scale features observed in a field of red neurons in TEp/TEO in M2 (cf Figure 3, section *c*). (*A*) Arrowheads indicate neurons in layer 2 with a quasi-regular spacing. Anterogradely labeled terminations from the injection of CTB-Alexa555 in TE are evident in layer 1. (*B*) Arrowhead indicates a clump of cells, oblique and vertical arrows indicate a horizontal and a vertical row of cells, respectively.

the projection foci expanded to include the sulcal depth. At these levels, the areas involved are likely to be IPa (depth), TEa (lower bank), and TEm (sulcal lip). Foci were relatively extensive, measuring 2.0–3.0 mm wide and up to about 4.0 mm AP. This is similar to what is described by Saleem et al. (2000) after more anterior injections, in TEad.

The number of labeled neurons and size of the projection foci were greatest in M2 and least in M3. Of particular note, the focus in IPa had a larger number of red neurons in both M1 and M2 (Table 2). In M1, we cannot preclude the possibility of an additional, anterior green focus (not included in the main tissue block). In M2, we were confident that anterior sections (600 µm distant) were devoid of any separate green focus, and we considered it likely that IPa is preferentially projecting to the red injection site. The foci in both IPa and TEa were partly composed of isolated fields of green or red neurons; but for about half their extent, green and red neurons were intermixed, and there were also some DL neurons. The TEa and TEm foci in M2 also included silver neurons (Table 2).

In some tissue sections, there was a clear side-by-side arrangement of red vs. green neurons (see Fig. 3, sections *b* and *c*). A definite topography was hard to establish, however, owing to the high degree of curvature in the STS and the complicated shapes of the individual areas.

Intraparietal Sulcus

In all 3 cases, labeled neurons occurred in the lower bank of the IPS. The projection focus was relatively delimited (shown only for M2 in Fig. 7 panel *d*; IPS of M3 is shown in Supplementary Fig. 5). In M1, with posterior and lateral injection sites, only a very few neurons were detected (estimated n = 20–50, adjusting for the 200-µm interval between scored sections), and for this reason strict quantification was not carried out in this brain. We identified the focus as probably being in the anterior portion of the lateral intraparietal area (aLIP) in M1.

The anterior injections in M2 and the posterior and medial injections in M3 produced more neurons, in what is probably aLIP and posterior anterior intraparietal area (AIP). The foci extended for 1.5–2.0 mm, in the lateral one-third of the IPS. In M2, the focus consisted of intermingled red and green neurons, and a few DL neurons. Some topographic organization was evident, such that at posterior levels, red was dominant (24 red vs. 8 green cells in section 219), but more anteriorly, green dominated (38 green vs. 12 red, sections 215, 211). Red neurons tended to occur deeper in the sulcus. Similarly, in M3, there was some topographic organization, with red cells located more anteriorly than green cells (Supplementary Fig. 5). These topographic trends reflect the relative disposition of the injection sites in both brains.

Prefrontal Cortex

All 3 brains had labeled neurons in the PFC (Fig. 7). Projection foci were relatively small (0.5 mm wide × 0.5–1.5 mm AP), but overall larger than the labeling in the IPS, in terms of extent and numbers of neurons. Foci consisted of intermixed neurons projecting to each injection site. DL neurons were apparent, as well as some triple-labeled neurons in M2 (Figs 7, 8).

Three distinct patches could be distinguished. These corresponded to 3 AP levels (respectively, *a*, *b*, and *c* in Fig. 7): 1) the anterior sector of the ventrolateral PFC (subdivisions of area 12), 2) the prearcuate convexity close to the IAS (area 45A, or the border of 45A and 46), and 3) the anterior bank of the IAS (areas 8/FEF and 45B). Possibly because of the gyral distortions in this region, there was no clear indication of topographic organization. In area 12, however, the labeling in M1 and M3 (with posterior injections) was concentrated laterally (12l), whereas the labeling in M2 (anterior injections) was situated more medially (12o). In both M2 and M3, labeling was anterior in area 12r.

Quantitative Analysis

For M1 and M2, quantitative analysis of the labeling in the occipital and temporal cortex was carried out (Table 2). For both brains, about the same total number of neurons were scored: 27 546 (M1) and 27 786 (M2). In M2, the percentage of red and green neurons was about equal (43% red, 50%

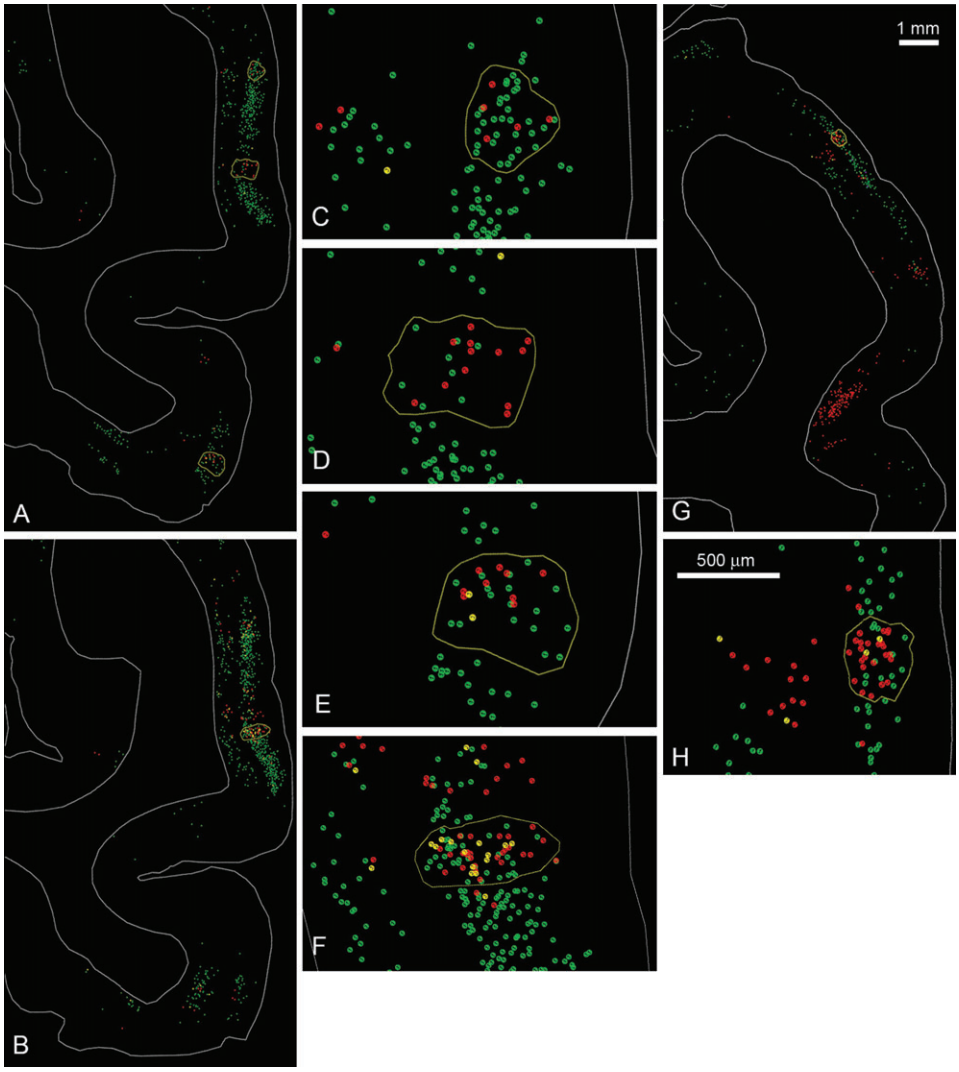

Figure 5. (*A* and *B*) Neurolucida chartings of retrogradely labeled neurons in M1 (partial coronal sections from below the STS), to illustrate "hotspots" (outlined areas). (*C–E*) Higher magnification of the outlined regions in (*A*). (*C*) Illustrates spot A in the surface view representation shown in Figure 6, (*D*) illustrates spot B, and (*E*) illustrates spot C from the surface view representation (Fig. 6). (*F*) From the outlined area in B, and corresponds to spot B in the surface view representation (Fig. 6). (*G*) Low magnification charting of a partial coronal section from M2. Outlined area corresponds to spot C in the surface view (Fig. 6), and is shown at higher magnification in (*H*). Scale bar in (G) applies also to (*A*) and (*B*). Scale bar in (*H*) applies to (*C–F*).

green); but in M1, the percentage of green neurons was higher (74% green; 21% red). This was a consequence of a larger portion of tissue (containing red neurons) being contained in the anterior, tangential block. The proportion of red and green neurons showed considerable variability, when subtotals were calculated by area. This was most clear for the STS (see IPa, TEa, TEm). Interestingly, area IPa in both brains had a higher number of red neurons and smaller number of green. Even in the regions of densest label, less than 50% of the neurons were labeled, as estimated by comparison with adjacent Nissl stained sections.

In the PFC for all 3 cases, a quantitative analysis was carried out (Table 3). In the anterior bank of the inferior arcuate sulcus (areas 8/FEF and 45B) of both M1 and M2 (but not M3), the number of red neurons exceeded that of green (i.e., same bias as for IPa). As the red injections in these 2 cases were both in TEpd, just anterior to PMTS, there may be a preferential connectivity between the inferior arcuate sulcus and this cortex, but this needs confirmation with a larger sample size. In 12l in M3, but not the other 2 brains, the number of red and green neurons was close to parity.

Double-labeled Cells

Calculated as a proportion of the total number, in aggregate, of red and green neurons, the proportion of DL neurons was low: 4.6% and 2% (of the red/green population) in M1 and M2, respectively. In some areas, however, the percentage of DL cells, was higher; namely, for IPa in the STS (6.5% and 5.9% DL red/green neurons in M1 and M2, respectively), and consistently about 7% of total neurons in the middle focus in PFC (45A/46 in M1 and M2, 45A/12l in M3). When recalculated as a separate proportion of red or green neurons, the percentage of DL neurons became significantly higher (see Table 2–3).

As described above, small foci of intermixed red, green, and DL neurons were identified in the posterior visual areas. In these "hotspots," the number of red and green neurons were closer to parity, and the percentage of DL neurons tended to be higher, especially for the supragranular layers. Calculated as

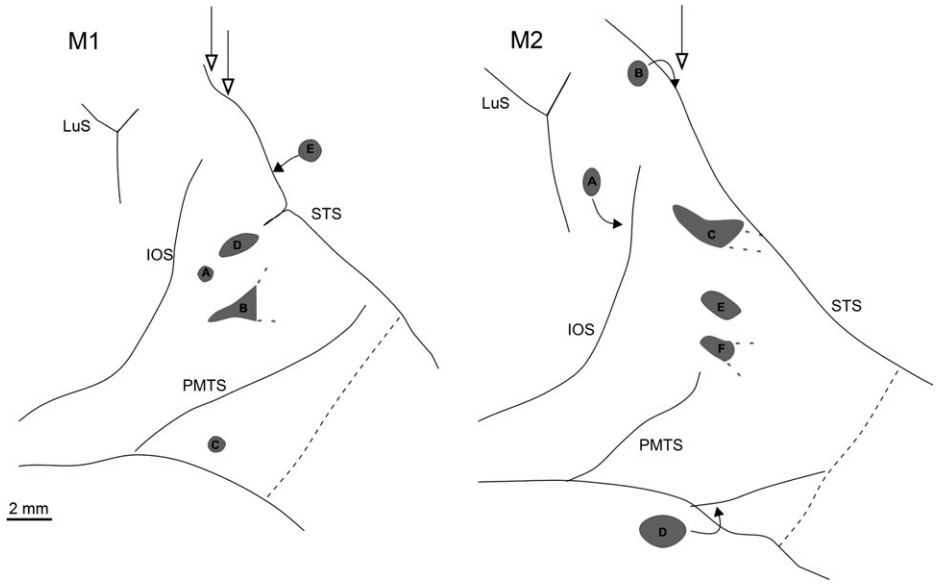

Figure 6. Schematic surface views depicting approximate size and location of hotspots (5 in M1 and 6 in M2). These are small regions where the number of red and green-labeled neurons were intermixed ("less imbalanced"), often including DL neurons (see text and Fig. 5). The actual number of red, green, and DL neurons are given in Table 4. Hollow arrows indicate the location of the sections shown in Figure 5, curved arrows indicate the approximate location of the hotspots in the ventral bank of STS or in the anterior bank of IOS. Grey dashes near hotspot B in M1 and hotspot C an F in M2 indicate that these hotspots continued anteriorly in single-color projection foci. Scale bar in M1 applies also to M2. Abbreviations and conventions as in Figures 1 and 2.

percentage of total number of labeled neurons, for 9 out of 11 identified hotspots, DL neurons commonly comprised 5–13% of the total number (Table 4). The number of DL neurons was smaller in the infragranular layers (6, 49, 0, 28, and 1 for Spots A–E in M1; and <11 for Spots A–E in M2).

The difference between hotspot and the adjacent neighboring cortex was quantitatively assayed using 3 criteria: 1) co-occurrence of red and green neurons; 2) balance of red and green cells (ratio of secondary/primary color $\geq$0.4); 3) presence of DL cells ($\geq$6%) (Supplementary Tables and Supplementary Fig. 4).

Layers

In area V4, neurons were predominantly located in the supragranular layers; but in all the other areas, the distribution was bilaminar. Notably, in the infragranular layers, neurons were distributed in both layers 5 and 6. A bilaminar distribution of projection neurons has been consistently reported from afferent connections after injections in TE or other association cortices (e.g., Morel and Bullier 1990; Baizer et al. 1991; Suzuki and Amaral 1994; Felleman et al. 1997; Saleem et al. 2000).

Other

As a gauge of the quality of label and size of injection sites, we examined label in several other structures. In all the 3 cases in the claustrum, there were abundant red- and green-labeled neurons (because of background in M2 and M3 silver neurons were not clearly visible in the subcortical structures). These formed 3–4 clusters, in approximately the same location in the ventral claustrum. Some DL neurons were found, but only a few (<5%). In the pulvinar, dense labeling occurred at posterior levels. This consisted of cells grouped in multiple, spatially separate clusters. Clusters were embedded in a wider field of scattered neurons. Only occasional DL cells could be found.

Discussion

Previous retrograde tracer experiments have described cortical projections to area TE from posterior unimodal visual areas (V4, TEO, and TEp); areas in the STS, IPS, PFC, and perirhinal and temporal polar cortex (Morel and Bullier 1990; Baizer et al. 1991; Webster et al. 1991, 1994; Martin-Elkins and Horel 1992; Suzuki and Amaral 1994; Saleem and Tanaka 1996; Saleem et al. 2000, 2008; and anterograde, Lavenex et al. 2002). Our results are consistent with these findings, and provide further information about the finer organization of this network. In particular, the small injections of multiple tracers reveal connectivity features that are both modular and distributed. These results, although based on a small sample size (3 monkeys), lay the groundwork for continued work with small injections in physiologically pretargeted domains, characterized in relation to face- or object-selectivity.

Previous anterograde tracer experiments of connections from TEO to TE revealed extensive axonal branching and multiple arbors in TE (Saleem et al. 1993). These findings are consistent with the occurrence of DL neurons. At least some single-labeled neurons, as discussed below, are also likely to have branched collaterals, but in this case, the collaterals are directed to one injected site and other, noninjected sites.

Convergence of Inputs

After large injections of retrograde tracers, earlier investigations reported a very widespread field of projection neurons in posterior visual areas (Morel and Bullier 1990; Baizer et al. 1991; Webster et al. 1991). The apparently large size of the projection fields, however, could have resulted from the injections involving multiple areas, in the adjoining STS and/or within area TE itself. This possibility now seems less likely, because comparably large fields resulted from the small injections used in the present experiments. The convergence from unimodal visual areas is slightly greater than what has

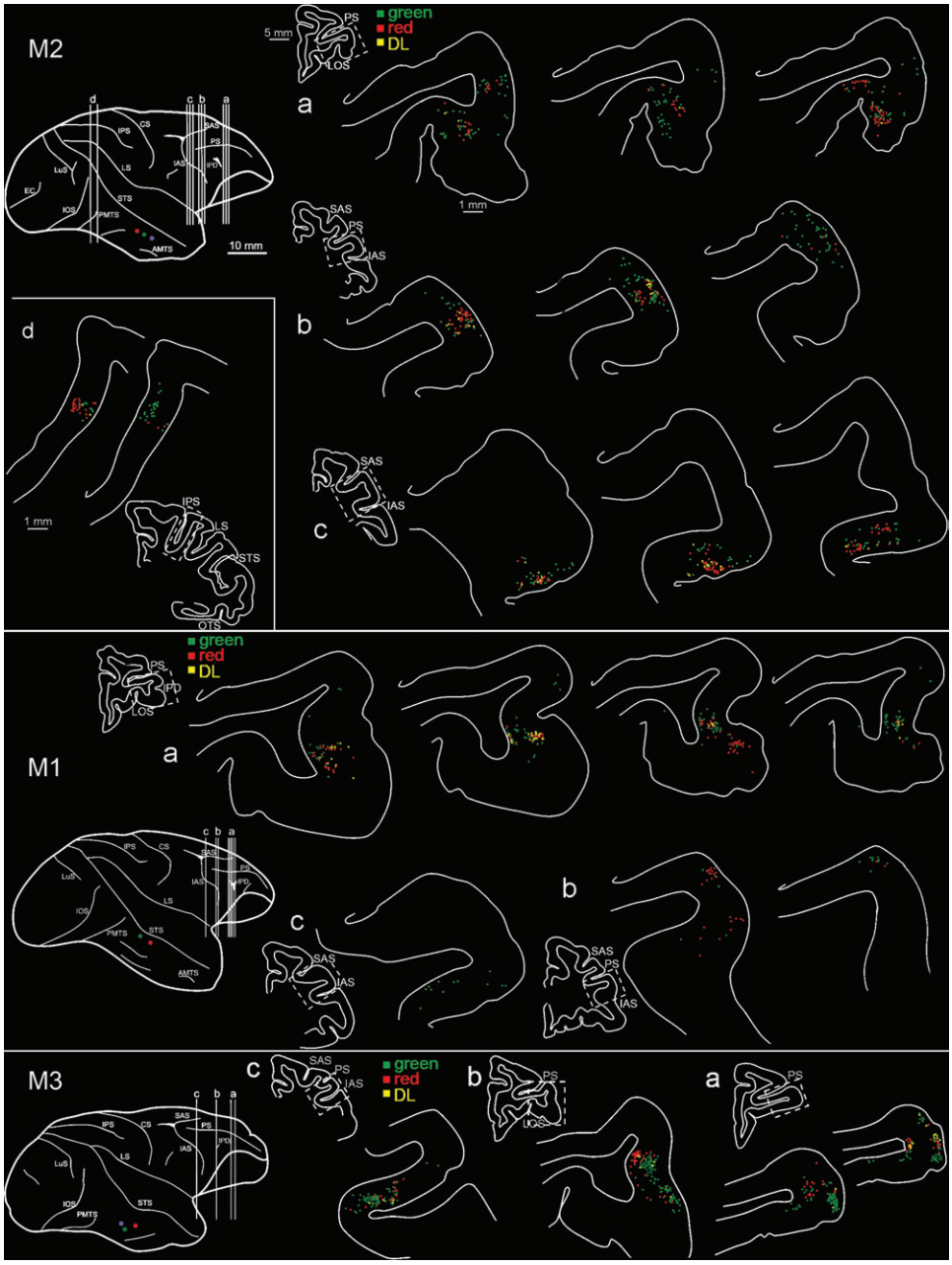

Figure 7. Drawings of representative coronal sections showing the distribution of retrogradely labeled neurons in the PFC (see the 3 repeated color codes for population scoring). Only for M2, labeling in the intraparietal cortex is also shown (level *d*). In all 3 brains, the prefrontal labeling was located at 3 rostrocaudal levels (*a*–*c*). For each level we choose from 1 to 4 representative sections (200 μm apart). Small section drawings are offset to the left for orientation, and the zone corresponding to the higher magnification chartings is indicated by the dashed boxes. The dorsolateral view of the injected hemispheres is repeated at the left, for further orientation. Silver neurons, which were very few in number, are not shown (but see Table 3). IPD = infraprincipal dimple; LOS = lateral orbital sulcus. Other abbreviations as in Figure 1.

been reported for V4 inputs to posterior TE (PITv), where retrogradely labeled neurons formed multiple clusters extending 2–3 mm dorso-ventrally and 1–3 mm AP in V4 (Felleman et al. 1997). A high degree of input convergence, as noted in Felleman et al. (1997), may be related to progressive increase in receptive field size and/or to mechanisms underlying attentional shifts across the visual scene.

Projection foci in the IPS and PFC were conspicuously smaller, about 0.5 mm wide and 1.0–3.0 mm in extent. This could be simply because areas in frontal and parietal cortex are themselves smaller. Alternatively, the smaller size may indicate functional differences in the types of connections. That is, both parietal and frontal connections to IT cortex have been categorized as "top-down," and these associational operations (as opposed to sensory, "bottom-up") may use a different spatial organization of projecting neurons.

Modular and Distributed

Recent fMRI studies in monkey have provided evidence for largely self-contained modular networks specialized for color or face processing (Conway et al. 2007; Moeller et al. 2008). In

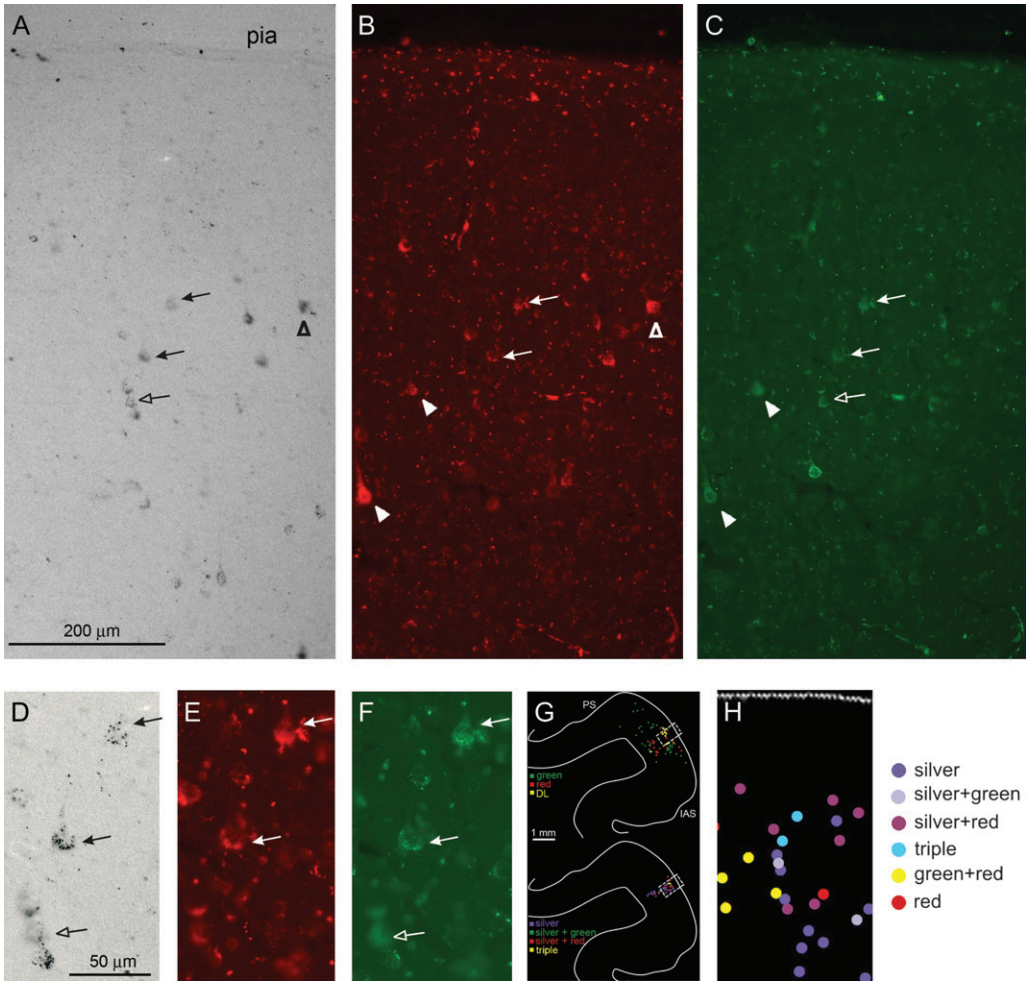

Figure 8. (*A–C*) Photomicrographs of labeled neurons in PFC in M2, (see Fig. 7, level *b*) showing silver (*A*), red (*B*), and green (*C*) neurons intermixed in the upper cortical layers. (*D*, *E*, *F*) Higher magnification from the central part of (*A*), (*B*), (*C*), respectively. Arrows indicate neurons labeled by multiple tracers: silver + red + green (solid arrows), silver + green (hollow arrow), silver + red (hollow arrowhead), red + green (solid arrowheads). (*G*) Partial section outline, to show the histological location of the labeled neurons. (*H*) Schematic re-mapping from the boxed zone in (*G*), corresponding to the photomicrographs in (*A–C*). *A*, *D* = bright field; *B*, *C*, *E*, *F* = fluorescent microscopy. Scale bar in *A* applies to *A–C*; scale bar in *D* applies to *D–F*. Abbreviations as in Figure 1.

the present experiments, we ascertained from optical imaging, with electrophysiological corroboration, that our injections corresponded to regions responsive to objects or to body-including-faces of animals and humans, but not specifically to face or color stimuli (Supplementary Figs 1 and 2). The resulting projections, we are proposing, have features of both a modular and distributed network.

All our injections resulted in multiple projection foci. These are reminiscent of 4 patches, activated by face stimuli in fMRI experiments, recently reported in areas likely to correspond to TEO, TE, and the STS (Tsao et al. 2008). In this respect, the input architecture is generally "modular". Each large projection patch, however, contains scattered neurons labeled from a different injection (i.e., a few red neurons in a green field, and vice versa). These would be missed in an fMRI experiment. Moreover, even in the densest fields of labeled neurons, only about 50% of the neurons were labeled. The intermixed, nonlabeled neurons could project to a different target (i.e., callosal connections) or to another, noninjected region within TE. Both these observations suggest some degree of intermixed, heterogeneous projection populations, and that would be more compatible with distributed processing.

Another proposal, consistent with our results, is that specifically face-selective patches are "embedded" in a large region of object-selective cortex (Tsao et al. 2003). Experiments at single cell anatomical resolution might resolve the debate, especially if combined with activity related functional markers (Luo et al. 2008).

Patches of face-selective neurons have been reported in macaque frontal lobe (Scalaidhe et al. 1999; Tsao et al. 2008). We note that all our injections (judged to be in object-related, not face-selective patches) resulted in 3 distinct projection foci in PFC; but a spatial match between the fMRI activations and our projection patches was suggested only for the patches identified as prefrontal arcuate (PA) and prefrontal lateral (PL) in fMRI (compare levels *c* and *a*, respectively, in Fig. 7). The orbital patch observed in fMRI had no equivalent in our results (but see Saleem et al. 2008), and our anterior patch, in 12r and 12o, seemed not to have any face-selective equivalent in the fMRI data.

Hotspots and Divergence

From axon reconstructions after injections of anterograde tracers in TEO, we know that terminations in TE often have

Table 4

Quantitative analysis of green, red and DL green/red cells in the hotspot regions (designated by A–E in M1 and A–F in M2)

M1						
Supragranular	Spot A	Spot B	Spot C	Spot D	Spot E	
Green	54	670	19	394	172	
Red	30	477	13	175	93	
DL	5	146	2	87	32	
Tot	89	1293	34	656	297	
%DL/tot	5.6%	11.3%	5.9%	13.3%	10.8%	
%DL/g	8.5%	17.9%	9.5%	18.1%	15.7%	
%DL/r	14.3%	23.4%	13.3%	33.2%	25.6%	
Infragranular						
Green	13	244	15	140	45	
Red	7	119	1	71	7	
DL	6	49	0	28	1	
Tot	26	412	16	239	53	
M2						
Supragranular	Spot A	Spot B	Spot C	Spot D	Spot E	Spot F
Green	45	28	299	213	89	73
Red	55	72	269	170	185	186
DL	5	2	53	8	15	17
Tot	105	102	621	391	289	276
%DL/tot	4.8%	2.0%	8.5%	2.0%	5.2%	6.2%
%DL/g	10.0%	6.7%	15.1%	3.6%	14.4%	18.9%
%DL/r	8.3%	2.7%	16.5%	4.5%	7.5%	8.4%
Infragranular						
Green	n.c.	3	99	90	25	21
Red	n.c.	6	146	123	64	93
DL	n.c.	0	11	0	1	2
Tot		9	256	213	90	116

Note: n.c. = not counted, because of sulcal distortion. Conventions as in Table 2.

multiple divergent arbors, separated by several mm (Fig. 7 in Saleem et al. 1993; Imura and Rockland 2005). This configuration would be expected to result in some neurons DL by the spatially separate injections. Perhaps more surprising are the scattered neurons within a projection focus to one injection, that project to a different injection, almost as if at random, or at least not according to any clear organization. These might be a subpopulation with single terminations directed to targets different from that of neighboring neurons in the same projection focus. Alternatively, they might have collateral terminations, but to other, noninjected sites in TE.

Also surprising, the use of multiple tracers revealed small patches ("hotspots") where the number of neurons projecting to different, spaced injections was more equal, and which often included DL neurons branching to both injections. A simple, technical explanation might be that these hotspots reflect overlap zones of the injection sites. This seems unlikely for several reasons. 1) With the exception of the green and silver injections in M3, the injection site haloes by visual inspection were clearly separated by at least 1.0 mm. 2) In the case of the 2 partially overlapping injections in M3, the number of DL neurons was consistently higher than in the hotspots. 3) DL neurons resulted from the red and silver injections in M2, which had the greatest spatial separation. 4) DL neurons occurred scattered outside hotspots.

Thus, another explanation is that hotspots are clusters where at least some neurons have a large number of branched collaterals. They may represent collections of neurons that preferentially project—by single arbors *or* by branched collaterals—to the particular sites injected in these cases. This raises the possibility of a complicated combinatorics of terminations, where neighboring neurons may have divergent, partially divergent, or convergent terminations onto the same postsynaptic domain (or column).

In IPS and PFC, the projection foci were smaller. This factor alone may have masked any comparable "hotspots." As it is, these foci as a whole were characterized by intermixing of neurons projecting to the different injections, along with DL neurons. If, as we are proposing, this organization is tightly related to axon collateral branching, then a corollary suggestion is that a high degree of divergent branching is a feature specific to association cortex. Further, we might speculate that "hotspots" within the posterior, unimodal visual areas are clusters of neurons with a functional architecture (divergence?) similar to that of a higher order association cortex.

In summary, our results suggest a complex connectivity network projecting to small domains within TE, with features that are both modular and distributed. Axon divergence may favor a distributed architecture, but more information is necessary concerning input convergence, specificity of postsynaptic targets, and physiological selectivity of the injection sites. Another question is to what degree intrinsic and extrinsic connections are organized according to similar principles. Anterograde tracing experiments have demonstrated a system of patchy intrinsic connections within TE (Fujita and Fujita 1996; Tanigawa et al. 2005), which, from investigations of intrinsic connections in other areas (e.g., Gilbert and Wiesel 1983), is derived from an extensive system of collaterals. How these relate to functional domains in TE remains a complex issue (Tanigawa et al. 2004).

Supplementary Material

Supplementary material can be found at: http://www.cercor.oxfordjournals.org/

Funding

RIKEN Brain Science Institute; and Grant-in-Aid for Scientific Research on Priority Areas "System study on higher order brain functions" and "Elucidation of neural network function in the brain" from the Ministry of Education, Culture, Sports, Science and Technology of Japan to N.I. (grant number: 18020032; 18500270).

Notes

We would like to thank H. Mashiko, Y. Abe, and D. Potapov for expert histological assistance, and J. Hyde for the help in figure preparation.
Conflict of Interest: None declared.

Address correspondence to Elena Borra, PhD, Dipartimento di Neuroscienze, Sezione di Fisiologia, Università di Parma, Via Volturno 39, I-43100 Parma, Italy. Email: elena.borra@nemo.unipr.it.

References

Baizer JS, Ungerleider LG, Desimone R. 1991. Organization of visual inputs to the inferior temporal and posterior parietal cortex in macaques. J Neurosci. 11:168–190.

Baylis GC, Rolls ET, Leonard CM. 1987. Functional subdivisions of the temporal lobe neocortex. J Neurosci. 7:330–342.

Bell AH, Hadj-Bouziane F, Frihauf JB, Tootell RB, Ungerleider LG. 2009. Object representations in the temporal cortex of monkeys and humans as revealed by functional magnetic resonance imaging. J Neurophysiol. 101:688–700.

Blatt GJ, Andersen RA, Stoner GR. 1990. Visual receptive field organization and cortico-cortical connections of the lateral intraparietal area (area LIP) in the macaque. J Comp Neurol. 299:421–445.

Borra E, Belmalih A, Calzavara R, Gerbella M, Murata A, Rozzi S, Luppino G. 2008. Cortical connections of the macaque anterior intraparietal (AIP) area. Cereb Cortex. 18:1094–1111.

Boussaoud D, Desimone R, Ungerleider LG. 1991. Visual topography of area TEO in the macaque. J Comp Neurol. 306:554–575.
Carmichael ST, Price JL. 1994. Architectonic subdivision of the orbital and medial prefrontal cortex in the macaque monkey. J Comp Neurol. 346:366–402.
Conway BR, Moeller S, Tsao DY. 2007. Specialized color modules in macaque extrastriate cortex. Neuron. 56:560–573.
Distler C, Boussaoud D, Desimone R, Ungerleider LG. 1993. Cortical connections of inferior temporal area TEO in macaque monkeys. J Comp Neurol. 334:125–150.
Fairhall SL, Ishai A. 2007. Effective connectivity within the distributed cortical network for face perception. Cereb Cortex. 17:2400–2406.
Felleman DJ, Xiao Y, McClendon E. 1997. Modular organization of occipito-temporal pathways: cortical connections between visual area 4 and visual area 2 and posterior inferotemporal ventral area in macaque monkeys. J Neurosci. 17:3185–3200.
Fujita I, Fujita T. 1996. Intrinsic connections in the macaque inferior temporal cortex. J Comp Neurol. 368:467–486.
Gerbella M, Belmalih A, Borra E, Rozzi S, Luppino G. 2007. Multimodal architectonic subdivision of the caudal ventrolateral prefrontal cortex of the macaque monkey. Brain Struct Funct. 212:269–301.
Gilbert CD, Wiesel TN. 1983. Clustered intrinsic connections in cat visual cortex. J Neurosci. 3:1116–1133.
Haxby JV, Hoffman EA, Gobbini MI. 2000. The distributed human neural system for face perception. Trends Cogn Sci. 4:223–233.
Ichinohe N, Sato T, Kurotani T, Tanifuji M, Rockland KS. 2008. In vivo imaging of connections in the monkey temporal cortex. Program No. 521.10. Society for Neuroscience 38th Annual Meeting. Washington DC.
Imura K, Rockland KS. 2005. Markedly different laminar distributions of single axons projecting from area TEO to anterior TE in macaque. Program No. 854.2 Society for Neuroscience 35th Annual Meeting. Washington DC.
Kobatake E, Tanaka K. 1994. Neuronal selectivities to complex object features in the ventral visual pathway of the macaque cerebral cortex. J Neurophysiol. 71:856–867.
Lavenex P, Suzuki WA, Amaral DG. 2002. Perirhinal and parahippocampal cortices of the macaque monkey: projections to the neocortex. J Comp Neurol. 447:394–420.
Li H, Fukuda M, Tanifuji M, Rockland KS. 2003. Intrinsic collaterals of layer 6 Meynert cells and functional columns in primate V1. Neuroscience. 120:1061–1069.
Livingstone MS, Hubel DH. 1984. Anatomy and physiology of a color system in the primate visual cortex. J Neurosci. 4:309–356.
Livingstone MS, Hubel DH. 1987. Connections between layer 4B of area 17 and the thick cytochrome oxidase stripes of area 18 in the squirrel monkey. J Neurosci. 7:3371–3377.
Logothetis NK. 2000. Object recognition: holistic representations in the monkey brain. Spat Vis. 13:165–178.
Logothetis NK, Pauls J, Poggio T. 1995. Shape representation in the inferior temporal cortex of monkeys. Curr Biol. 5:552–563.
Luo L, Callaway EM, Svoboda K. 2008. Genetic dissection of neural circuits. Neuron. 57:634–660.
Luppino G, Rozzi S, Calzavara R, Matelli M. 2003. Prefrontal and agranular cingulate projections to the dorsal premotor areas F2 and F7 in the macaque monkey. Eur J Neurosci. 17:559–578.
Martin-Elkins CL, Horel JA. 1992. Cortical afferents to behaviorally defined regions of the inferior temporal and parahippocampal gyri as demonstrated by WGA-HRP. J Comp Neurol. 321:177–192.
Moeller S, Freiwald WA, Tsao DY. 2008. Patches with links: a unified system for processing faces in the macaque temporal lobe. Science. 320:1355–1359.
Morel A, Bullier J. 1990. Anatomical segregation of two cortical visual pathways in the macaque monkey. Vis Neurosci. 4:555–578.
Orban GA. 2008. Higher order visual processing in macaque extrastriate cortex. Physiol Rev. 88:59–89.
Pasupathy A. 2006. Neural basis of shape representation in the primate brain. Prog Brain Res. 154:293–313.
Rockland KS, Pandya DN. 1981. Cortical connections of occipital lobe in the rhesus monkey: interconnections between areas 17,18,19 and the superior temporal sulcus. Brain Res. 212:249–270.
Saleem KS, Kondo H, Price JL. 2008. Complementary circuits connecting the orbital and medial prefrontal networks with the temporal, insular, and opercular cortex in the macaque monkey. J Comp Neurol. 506:659–693.
Saleem KS, Suzuki W, Tanaka K, Hashikawa T. 2000. Connections between anterior inferotemporal cortex and superior temporal sulcus regions in the macaque monkey. J Neurosci. 20:5083–5101.
Saleem KS, Tanaka K. 1996. Divergent projections from the anterior inferotemporal area TE to the perirhinal and entorhinal cortices in the macaque monkey. J Neurosci. 16:4757–4775.
Saleem KS, Tanaka K, Rockland KS. 1993. Specific and columnar projection from area TEO to TE in the macaque inferotemporal cortex. Cereb Cortex. 3:454–464.
Sato T, Uchida G, Tanifuji M. 2008. Cortical columnar organization is reconsidered in inferior temporal cortex. Cereb Cortex. PMID: 19068487.
Scalaidhe SP, Wilson FA, Goldman-Rakic PS. 1999. Face-selective neurons during passive viewing and working memory performance of rhesus monkeys: evidence for intrinsic specialization of neuronal coding. Cereb Cortex. 9:459–475.
Seltzer B, Pandya DN. 1978. Afferent cortical connections and architectonics of the superior temporal sulcus and surrounding cortex in the rhesus monkey. Brain Res. 149:1–24.
Shipp S, Zeki SM. 1985. Segregation of pathways leading from area V2 to area V4 and V5 of macaque monkey visual cortex. Nature. 315:322–325.
Sincich LC, Horton JC. 2002. Pale cytochrome oxidase stripes in V2 receive the richest projection from macaque striate cortex. J Comp Neurol. 447:18–33.
Sincich LC, Jocson CM, Horton JC. 2007. Neurons in V1 patch columns project to V2 thin stripes. Cereb Cortex. 17:935–941.
Suzuki WA, Amaral DG. 1994. Perirhinal and parahippocampal cortices of the macaque monkey: cortical afferents. J Comp Neurol. 350:497–533.
Tanaka K. 1996. Inferotemporal cortex and object vision. Annu Rev Neurosci. 19:109–139.
Tanigawa H, Rockland KS, Tanifuji M. 2004. Relationship between horizontal connections and functional structure revealed by intrinsic signal imaging, unit recording, and anatomical tracing in macaque anterior inferotemporal cortex (area TE). Program No. 300.11. Society for Neuroscience 34th Annual Meeting. San Diego, CA.
Tanigawa H, Wang Q, Fujita I. 2005. Organization of horizontal axons in the inferior temporal cortex and primary visual cortex of the macaque monkey. Cereb Cortex. 12:1887–1899.
Tsao DY, Freiwald WA, Knutsen TA, Mandeville JB, Tootell RB. 2003. Faces and objects in macaque cerebral cortex. Nat Neurosci. 6:989–995.
Tsao DY, Livingstone MS. 2008. Mechanisms of face perception. Annu Rev Neurosci. 31:411–437.
Tsao DY, Schweers N, Moeller S, Freiwald WA. 2008. Patches of face-selective cortex in the macaque frontal lobe. Nat Neurosci. 11:877–879.
Tsunoda K, Yamane Y, Nishizaki M, Tanifuji M. 2001. Complex objects are represented in macaque inferotemporal cortex by the combination of feature columns. Nat Neurosci. 4:832–838.
Ungerleider LG, Galkin TW, Desimone R, Gattass R. 2008. Cortical connections of area V4 in the macaque. Cereb Cortex. 18:477–499.
Wang G, Tanifuji M, Tanaka K. 1998. Functional architecture in monkey inferotemporal cortex revealed by in vivo optical imaging. Neurosci Res. 32:33–46.
Webster MJ, Bachevalier J, Ungerleider LG. 1994. Connections of inferior temporal areas TEO and TE with parietal and frontal cortex in macaque monkeys. Cereb Cortex. 4:470–483.
Webster MJ, Ungerleider LG, Bachevalier J. 1991. Connections of inferior temporal areas TE and TEO with medial temporal-lobe structures in infant and adult monkeys. J Neurosci. 11:1095–1116.
Yukie M, Takeuchi H, Hasegawa Y, Iwai E. 1990. Differential connectivity of inferotemporal area TE with the amygdala and the hippocampus in the monkey. In: Iwai E, Mishkin M, editors. Vision, memory, and the temporal lobe. New York: Elsevier. p. 129–135.
Zeki S. 1996. Are areas TEO and PIT of monkey visual cortex wholly distinct from the fourth visual complex (V4 complex)? Proc Biol Sci. 263:1539–1544.
Zeki SM, Shipp S. 1989. Modular connections between areas V2 and V4 of macaque monkey visual cortex. Eur J Neurosci. 1:494–506.